Three-Chromophore Excited-State Mixed Valence

ARTICLE *in* THE JOURNAL OF PHYSICAL CHEMISTRY A · JANUARY 2009

Impact Factor: 2.69 · DOI: 10.1021/jp807940h · Source: PubMed

THE JOURNAL OF PHYSICAL CHEMISTRY A

Article

Three-Chromophore Excited-State Mixed Valence

Ryan M. Hoekstra, Marcelle M. Dibrell, Michael N. Weaver, Stephen F. Nelsen, and Jeffrey I. Zink

J. Phys. Chem. A, **2009**, 113 (2), 456-463 • DOI: 10.1021/jp807940h • Publication Date (Web): 22 December 2008

Three-Chromophore Excited-State Mixed Valence

Ryan M. Hoekstra,[†] Marcelle M. Dibrell,[†] Michael N. Weaver,[‡] Stephen F. Nelsen,*[,‡] and Jeffrey I. Zink*[,†]

Department of Chemistry and Biochemistry, University of California, Los Angeles, California 90095, and Department of Chemistry, University of Wisconsin, Madison, 1101 University Avenue, Madison, Wisconsin 53706-1396

Received: September 7, 2008; Revised Manuscript Received: October 25, 2008

The lowest energy optical electronic absorption band of the three-chromophore system tris(4-bromophenyl)-amine radical cation is analyzed. The lowest energy electronic transition corresponds to a *p*-bromophenyl orbital to nitrogen p orbital transition that places the positive charge on three equivalent *p*-bromophenyl chromophores. The excited electronic state is an example of excited-state mixed valence (ESMV), and the spectrum is interpreted using two ESMV models. The simplest model invokes the concept of an "effective coupling" between the three identical chromophores with an excited-state energy splitting equal to three times the coupling. A more accurate model, the "neighboring orbital model", utilizes the coupling between the bridge's and charge-bearing unit's orbitals closest in energy. The three-chromophore system provides a striking illustration of the failure of an effective coupling term to account for ESMV splitting. The calculated relative energies of the diabatic and adiabatic states are different, but the calculated absorption spectra of the two models show nearly identical vibrational fine structure. Resonance Raman data and the time-dependent theory of electronic and resonance Raman spectroscopies are used to calculate the spectra.

Introduction

Excited-state mixed valence (ESMV) molecules have two or more identical charge-bearing units - or chromophores - with different oxidation levels in the electronic excited state and a symmetric charge distribution in the ground state. In previous work, mixed valence compounds with two charge-bearing units have been studied.[1] The charge-bearing units (M) are coupled through a bridging group (B). The optical absorption spectrum and resonance Raman intensities can be successfully described by a pair of coordinate displaced harmonic oscillators coupled to each other. The coupling in this model is the effective coupling between the two charge-bearing units arising from their interaction through the bridge. The magnitude of the coupling determines the extent of localization or delocalization in the excited state, and the "hopping" rate of the charge in the delocalized limit.

Many mixed valence compounds have been reported in which there are three,[2−6] four,[7−10] or six[10−17] symmetrically displaced charge-bearing units coupled to each other through a bridging group. In this work, three charge-bearing units are considered where the charge is located on the bridging unit in the ground state and can be represented as $^{+}BM_3$. Upon optical excitation the charge is pushed by the oscillating electric vector of light onto a chromophore and can be represented as $M^{+}BM_2$. The magnitude of the coupling between the chromophores determines the extent to which the charge will either localize onto a single chromophore or delocalize over the three chromophores.

Wieland showed in 1907 that tris(para)-substituted triarylamines gave isolable oxidation products,[18] and they were first correctly identified as radical cation salts by Weitz and Schwechten in 1926.[19] Important work on substituted triarylamines and their radical cations was carried out by Walter and co-workers,[20] who improved syntheses, studied spectra, and obtained the first X-ray structure of a triarylamine radical cation derivative, the tris-*p*-phenyl compound.[20j] Triarylaminium salts are among the more potent storable single-electron oxidants;[21] the tris(4-bromophenyl)amine hexachloroantiminate [$N(p\text{-}C_6H_4Br)_3]^{+}SbCl_6^{-}$ has proven to be a useful synthetic reagent.[22]

In the ground electronic state of $[N(p\text{-}C_6H_4Br)_3]^{+}$, the charge is centered on the nitrogen atom with significant charge delocalization as elucidated by ESR spectroscopy. Electron delocalization from a nitrogen radical cation toward an aryl group will introduce spin onto the aryl group carbons, and the approximate proportionality between spin density and ESR splitting constant for planar nitrogens and aryl hydrogens provides a way to assess the charge distribution in the radical cation. An accurate nitrogen ESR splitting constant has apparently not been reported for the bromo-substituted compound as its ESR spectrum is especially broadened.[20d] The splitting constant for the chloro analogue is 9.62 gauss,[23] corresponding to a spin density of about 0.38 at nitrogen. The ortho hydrogen ESR splitting constants have been measured at 2.10 G for the *p*-Cl and 2.04 G for the *p*-Br compounds,[20h] corresponding to spin densities of about 0.09. These ESR splitting constants imply significant delocalization of spin and thus charge onto the three aryl rings in the radical cation ground state, but less spin on each aryl ring than on the bridging nitrogen. Upon excitation more charge is pushed onto the *p*-bromoaryl groups.

In this paper an effective coupling model and a neighboring orbital model are introduced to describe the excited-state mixed valence transition. The effective coupling model consists of three displaced harmonic oscillators coupled directly to each other, representing the three chromophores. The coupling is an effective coupling arising from the interaction of the three chromophores with each other through the bridge. The bridge is represented by a single harmonic oscillator centered at the electronic origin energetically displaced from the mixed valence

* To whom correspondence should be addressed.
[†] University of California.
[‡] University of Wisconsin.

10.1021/jp807940h CCC: $40.75
Published on Web 12/22/2008

state. In the neighboring orbital model three displaced harmonic oscillators, representing the chromophores, are coupled to an energetically displaced harmonic oscillator, representing the bridge. The three chromophores are not coupled directly to each other, but the charge-bearing units are still able to communicate with each other through the bridge. The spectra for each model are calculated using the time-dependent theory of spectroscopy.[24−27]

Numerical and Theoretical Methods. TD-DFT and Koopmans-based calculations were performed to assign the bands observed in the optical absorption spectrum of $[N(p\text{-}C_6H_4Br)_3]^+$. The possible single-electron transitions are identified using Hoijtink-type designations:[28,29] type A transitions are β ("filled") $\rightarrow \beta$ SOMO, type B are α SOMO $\rightarrow \alpha$ (virtual), and type C for all other transitions. Transitions from both filled and virtual orbitals are numbered as their energy separation from the SOMO increases. In Koopmans-based calculations[30−33] transitions are assigned using neutral at the radical cation geometry (NCG) for the type A transitions, and dication at the radical cation geometry (DCG) for the type B transitions. The lowest energy transitions of radical cations are often type A, with little configuration interaction (CI) mixing. The next large band is often type B, with higher amounts of CI mixing corresponding to the greater transition energy. Koopmans-based calculations often produce values that are closer to the observed transition energies than do TD-DFT calculations, despite the fact that Koopmans-based calculations ignore CI. Vibrational calculations were performed on the optimized radical cation to assign the Raman modes. All calculations were carried out in the Gaussian 03 suite using the B3LYP/6-31G* method and basis set.[34]

Time-Dependent Theory: Calculation of the Electronic Absorption Spectrum for Three Chromophores. The fundamental equation for the calculation of an absorption spectrum in the time-dependent theory is

$$I(\omega) = C\omega \int_{-\infty}^{+\infty} \exp(i\omega t)\left\{\langle\Phi|\Phi(t)\rangle \times \exp\left(-\Gamma^2 t^2 + \frac{iE_0}{h}t\right)\right\} \mathrm{d}t \qquad (1)$$

with $I(\omega)$ as the absorption intensity at frequency ω, E_0 the energy of the electronic transition at the origin, and Γ a phenomenological damping factor that accounts for relaxation into other vibrational modes of the molecule and to the "bath".[24a−c] The effect of increasing Γ is that the resolution of the absorption spectrum decreases, thereby broadening out vibrational fine structure. The most important portion of eq 1 is $\langle\Phi|\Phi(t)\rangle$, the autocorrelation function of the wave packet (Φ) prepared on the excited-state potential surfaces after the optical electronic transition, with the wave packet developing on the surface in time ($\Phi(t)$). In the absence of coupling, the total autocorrelation function in a system with K coordinates is given as

$$\langle\Phi|\Phi(t)\rangle = \prod_{k=1}^{K} \langle\varphi^k|\varphi^k(t)\rangle \qquad (2)$$

where φ^k is the wave packet associated with coordinate k (k = 1,..., K). In the following section only a single coordinate will be considered, eliminating the index k for clarity.

In the effective coupling model the $t = 0$ wave packet is defined as

$$\varphi(X, Y, j, t=0) = \sum_{j=1}^{3} \mu_j \chi_i(X, Y) \qquad (3)$$

where χ_i denotes the lowest energy eigenfunction of the ground-state surface. The ground-state eigenfunction is multiplied by the transition dipole moment, μ_j. The sign of μ_j depends on the direction of the electron transfer and is determined by orientational averaging.[35] The dipole moments are discussed later on in section 6.

In the effective coupling model three coupled surfaces, representing the excited state, are involved, and it is necessary to keep track of the three wave packets φ_j (j = 1, 2, 3) moving on the coupled potential surfaces.[36] The wave packet $\varphi_j(t)$ is given by the time-dependent Schrödinger equation:

$$i\frac{\partial}{\partial t}\begin{pmatrix}\varphi_1\\ \varphi_2\\ \varphi_3\end{pmatrix} = \begin{pmatrix}H_1 & H_{\mathrm{eff}} & H_{\mathrm{eff}}\\ H_{\mathrm{eff}} & H_2 & H_{\mathrm{eff}}\\ H_{\mathrm{eff}} & H_{\mathrm{eff}} & H_3\end{pmatrix}\begin{pmatrix}\varphi_1\\ \varphi_2\\ \varphi_3\end{pmatrix} \qquad (4)$$

H_{eff} is the coupling between the diabatic potentials. The diagonal elements H_j of the total Hamiltonian are given as

$$H_j = -\frac{1}{2M}\nabla^2 + V_j(X, Y) \qquad (5)$$

The gradient term is the nuclear kinetic energy and $V_j(X, Y)$ is the potential energy as a function of the configurational coordinate given as

$$V_1(X, Y) = \frac{1}{2}k[(X-\Delta)^2 + Y^2]$$

$$V_{2,3}(X, Y) = \frac{1}{2}k\left[\left(X + \frac{1}{2}\Delta\right)^2 + \left(Y \pm \frac{\sqrt{3}}{2}\Delta\right)^2\right] \qquad (6)$$

The force constant is defined as $k \equiv 4\pi^2 M(h\omega_j)^2$, and Δ is the displacement of the potential minimum along the configurational coordinate. Although harmonic potentials are chosen for simplicity, the functional form of V_j is not restricted by the model.

In the neighboring orbital model the spectra are calculated using eq 1. The $t = 0$ wave packet is defined as

$$\varphi(X, Y, j, t=0) = \sum_{j=1}^{4} \mu_j \chi_i(X, Y) \qquad (7)$$

The ground-state eigenfunction of the coupled system is given as χ_i. The ground-state wave packet is multiplied by the transition dipole moments discussed later. It is necessary to keep track of four wave packets φ_j (j = 1, 2, 3, 4) moving on the coupled potential surfaces. The wave packet $\varphi_j(t)$ is given by the time-dependent Schrödinger equation:

$$i\frac{\partial}{\partial t}\begin{pmatrix}\varphi_1\\ \varphi_2\\ \varphi_3\\ \varphi_4\end{pmatrix} = \begin{pmatrix}H_1 & V & V & V\\ V & H_2 & 0 & 0\\ V & 0 & H_3 & 0\\ V & 0 & 0 & H_4\end{pmatrix}\begin{pmatrix}\varphi_1\\ \varphi_2\\ \varphi_3\\ \varphi_4\end{pmatrix} \qquad (8)$$

V is the coupling between the bridge diabat, H_1, and the chromophore diabats, H_j (j = 2, 3, 4). The diagonal elements H_j are defined according to eq 5. The potential energy as a functional form of the configurational coordinate is given as

$$V_1(X, Y) = \frac{1}{2}k[X^2 + Y^2] + E_{\mathrm{B}}$$

$$V_2(X, Y) = \frac{1}{2}k[(X-\Delta)^2 + Y^2] + E_{\mathrm{M}}$$

$$V_{3,4}(X, Y) = \frac{1}{2}k\left[\left(X + \frac{1}{2}\Delta\right)^2 + \left(Y \pm \frac{\sqrt{3}}{2}\Delta\right)^2\right] + E_{\mathrm{M}} \qquad (9)$$

k and Δ are the same as defined earlier, and E_{B} and E_{M} are the energies of the potential minimum for the bridge and chromophore states, respectively.

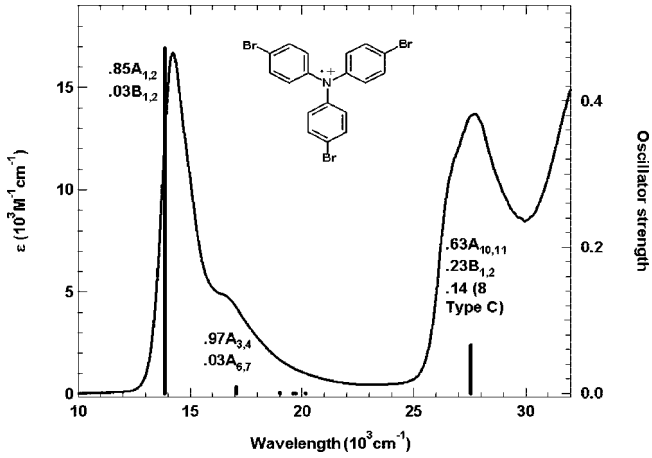

Figure 1. Absorption spectrum of $[N(p\text{-}C_6H_4Br)_3]^+$ in acetonitrile, compared with TD-DFT calculations, given by the vertical lines.

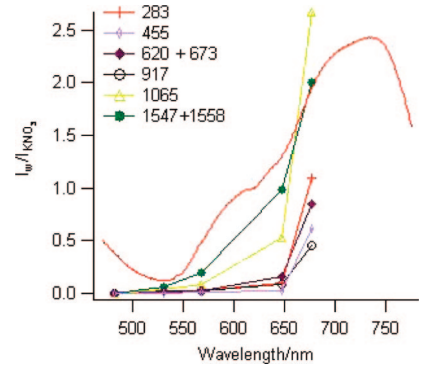

Figure 2. Absorbance profile of $[N\text{-}(p\text{-}C_6H_4Br)_3]^+$ in KBr, shown by the solid line, and the resonance Raman excitation profiles of selected modes relative to the 1050 cm^{-1} mode of KNO_3, given by the points connected by lines. The relative intensities of the two modes near 650 and 1550 cm^{-1} have been added together for clarity.

The ground-state eigenfunction is found using

$$\chi_i = \text{const} \int_0^T \eta(t)\, w(t) \exp\left[\frac{iE_i t}{h}\right] dt \qquad (10)$$

where χ_i is the ground-state eigenfunction corresponding to the eigenvalue E_i, $\eta(t)$ is the propagating wave function initially located arbitrarily on the surface, and $w(t)$ is a Hanning window function. Note that for coupled potentials, as in the neighboring orbital model, the ground-state eigenfunction is an array with four components corresponding to the four diabatic potentials composing the basis of the calculations.

Results and Discussion

1. Electronic Absorption Spectrum. The absorption spectrum of $[N(p\text{-}C_6H_4Br)_3]^+$ and the band assignments using TD-DFT are shown in Figure 1. The results are summarized in Table 1, along with Koopmans-based calculations. The low-energy band at 13 700 cm^{-1} is assigned as the HOMO to SOMO transition ($A_{1,2}$). This transition is the one that will be modeled as a mixed valence transition. The shoulder occurring at about 15 800 cm^{-1} is assigned as a transition from the nonbonding aryl orbitals ($A_{3,4}$) to the SOMO. The band with a maxium about 27 200 cm^{-1} is assigned as a complex transition involving considerable configuration interaction, including contributions from the e pair of single-node aryl orbitals having overlap with the nitrogen p lone pair to the SOMO($A_{10,11}$), the SOMO to LUMO transition ($B_{1,2}$), and eight type C transitions (see section 3 for MO drawings).

2. Raman Spectra and Excited-State Distortions. Raman spectra were collected both in and out of resonance with the lowest energy absorption band. Figure 2 shows the Raman intensities measured using 482.9, 530.9, 568.2, 647.1, and 676.4 nm laser excitation wavelengths; the absorption profile in KBr is shown revealing that the enhancement profile follows the absorption profile. The Raman spectra were collected in KNO_3, and the absorption spectrum was collected in KBr; these two salts typically have similar solvatochromic shifts. The distortions of the enhanced vibrations are calculated using Savin's formula with KNO_3 as the internal standard; the values are used to estimate the distortions employed in calculating the electronic absorption spectrum in section 7, reported in Table 2. The distortions can be interpreted as mode-specific reorganization energies, using the relationship $\lambda_q = (1/2)\Delta^2\omega$, which results in a vibrational reorganization energy of 600 cm^{-1}; the calculated reorganization energy using B3LYP/6-31G* is 1109 cm^{-1} including a 57 cm^{-1} mode comprising about half of the reorganization energy.[37] Vibrational assignments were made using the frequency calculations described in the numerical methods section.

3. Gaussian Calculated Molecular Orbital Diagram. The Koopmans-based calculations were used to make the molecular orbital diagram of $[N(p\text{-}C_6H_4Br)_3]^+$, shown in Figure 3. The diabatic orbitals used to describe the excited-state mixed valence transition ($A_{1,2}$) are the antibonding combination of the aryl and bromine (H_{π^*}) and the nitrogen p_z orbital (H_N). The totally symmetric linear combination of the H_{π^*} orbitals interacts with the bridge giving two totally symmetric molecular orbitals (H_3^A H_2^A); these two totally symmetric molecular orbitals and the doubly degenerate molecular orbital pair ($H_{\pi^*}^E$) are described by the adiabatic surfaces in both the effective coupling and neighboring orbital model, *vide infra*.

TABLE 1: Comparison of Calculated Absorption Bands for $(p\text{-}C_6H_4Br)_3N$ Radical Cation ((U)B3LYP/6-31G*, D_3 Symmetry, a_2 SOMO)

obsvd in CH_2Cl_2	TD-DFT (10 transitions)		Koopmans-based	
$h\nu$, cm^{-1} (ε M^{-1} cm^{-1})	$h\nu$, cm^{-1} (f [a])	assignment	$h\nu$, cm^{-1} (f [a])	assignment
(1) 13 700 (31 000)	13 870 (0.472)	0.85 $A_{1,2}$, 0.03 $B_{1,2}$	12 500 (0.280)	$A_{1,2}$ e
sh[b] ~15 800 (8100)	17 070 (0.009)	0.97 $A_{3,4}$, 0.03 $A_{6,7}$	16 660 (0.002)	$A_{3,4}$ e
	19 010 (0.0012)	1.00 A_9	18 540 (0.003)	A_5 a_1
	19 600 (0.0000)	0.97 A_5, 0.02 A_8	20 750 (0.000)	A_6 a_2
	19 710 (0.0001)	0.97 $A_{3,4}$, 0.03 $A_{6,7}$	21 670 (0.000)	A_7 a_2
	20 160 (0.0000)	0.94 A_8, 0.015 A_5[c]	21 680 (0.000)	$A_{8,9}$ e
(2) 27 200 (20 100)	27 540 (0.066)	0.63 $A_{10,11}$, 0.23 $B_{1,2}$[d]	28 430(0.000)	$A_{10,11}$ e
			30 060 (0.202)	$B_{1,2}$ e

[a] Oscillator strength. [b] Shoulder. [c] Also a contribution of 0.015 B_6. [d] Also a total contribution of 0.14 for eight type C bands, none greater than $f = 0.021$.

TABLE 2: Observed Resonance Raman Frequencies and Intensities and Calculated Distortions and Assignments[a]

ω^b	ω^c	Δ^d	Δ^e	$\lambda_q{}^f$	assignment[g]
171	156	0.75	0.70	42	molecular stretch (a_1)
282	280	0.80	0.80	90	ring rocking (e)
404	416	0.26	0.20	8	ring rocking (e)
454	455	0.37	0.40	36	molecular stretch (a_1)
511	526	0.18	0.15	6	ring breathing/N−Ar scissors (e)
618	633	0.23	0.30	28	ring breathing (e)
672	686	0.21	0.83	230	ring breathing/N−Ar scissors (e)
810	837	0.25	0.25	25	out of plane Ar−H bend (e)
917	932	0.16	0.10	4	Ar−N−Ar scissors bend (e)
1001	1025	0.10	0.10	5	in plane ring breathing (a_1)
1065	1096	0.33	0.40	85	Ar−Br stretch, ring breathing (a_1)
1172	1198	0.16	0.20	23	Ar−N stretch (a_1)
1547	1586	0.16	0.10	8	ring stretch (e)
1558	1613	0.12	0.10	8	ring Stretch (e)

[a] All frequencies and energies are given in cm^{-1}. [b] Measured frequency. [c] Gaussian calculated frequency. [d] Distortions from Savin's formula. [e] Distortions from spectral fit. [f] Reorganization energy, using distortions from spectral fit. [g] Symmetry assignment

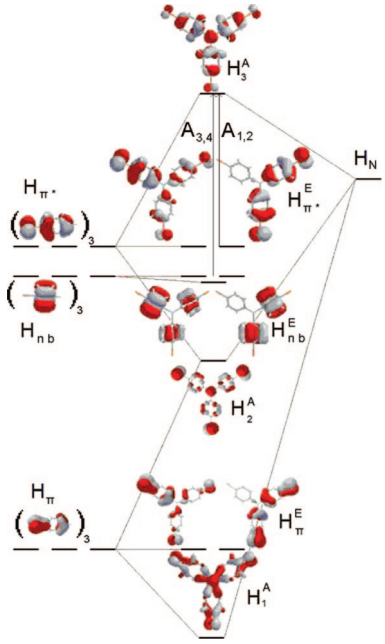

Figure 3. Calculated neighboring orbital model with the two lowest energy transitions, $A_{1,2}$ $A_{3,4}$. The labels of the diabatic states are shown above and below the figures; the labels of the adiabatic states are shown alongside. All of the molecular orbitals are filled except for the highest energy orbital ($H_3{}^A$), which is the SOMO. The totally symmetric linear combination of the nonbonding aryl orbitals ($H_{nb}{}^A$) is not shown.

The nonbonding aryl orbitals (H_{nb}) are not of appropriate symmetry to interact with the bridging nitrogen; the shoulder at ~15 800 cm^{-1} is attributed to the transition from the nonbonding orbitals to the SOMO ($A_{3,4}$). The unexpected nodal pattern on the aryl group of orbital $H_2{}^A$ arises from a contribution of the bonding combination between the aryl and bromine (H_π) in addition to H_{π^*} and H_N.

4. "Effective Coupling" Model. The lowest energy transition can be modeled as a charge transfer from the bridging nitrogen atom (B) to the aryl groups (M). The ground state is represented by a single harmonic oscillator centered at the electronic origin (H_N). The excited state, corresponding to the electron transfer from the three *p*-C_6H_4Br charge-bearing units (H_{ArBr}) to the nitrogen, is represented by three degenerate harmonic potential

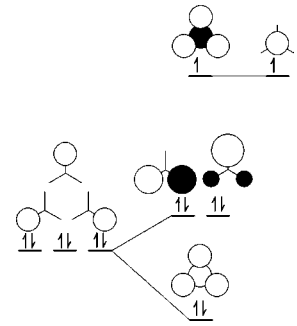

Figure 4. Simplified molecular orbital diagram for the effective coupling model. The bridge does not mix with the chromophore orbitals and remains energetically equivalent to the diabatic bridge state. The three chromophores couple to each other splitting the E and A states from the diabatic energies by $-H_{eff}$ and $+2H_{eff}$, respectively. The ground-state electron configuration is shown for both the diabatic and adiabatic basis.

energy surfaces displaced from the electronic origin according to the C_3 point group. The excited-state diabats are energetically displaced from the ground state. The three harmonic oscillators are coupled directly to each other as seen in $\mathbf{H}_{e.c.}$ (eq 11), since they are allowed to interact through the bridge. The coupling can be described as the effective coupling (H_{eff}) between the three charge-bearing units.

$$\mathbf{H}_{e.c} = \begin{bmatrix} H_N & 0 & 0 & 0 \\ 0 & H_{ArBr} & H_{eff} & H_{eff} \\ 0 & H_{eff} & H_{ArBr} & H_{eff} \\ 0 & H_{eff} & H_{eff} & H_{ArBr} \end{bmatrix} \qquad (11)$$

The effective coupling between the three excited-state diabats serves to split the excited state into three adiabatic states, as shown in Figure 4. The three adiabatic states are separated in energy by three times the effective coupling. Two of the adiabatic states are degenerate at the electronic origin and are displaced from the diabatic energy by $-H_{eff}$. The two degenerate adiabats represent the E electronic state, which has a dipole allowed electronic transition from the ground state. The third adiabatic state representing the A excited electronic state is displaced from the diabatic energy by $2H_{eff}$. The transition from the ground state to the A excited state is dipole forbidden but vibronically allowed.

5. Neighboring Orbital Model. The neighboring orbital model for the three chromophore system can be written using only the frontier molecular orbitals of the bridge and chromophore system. The bridging group - in this case the p_z orbital of the nitrogen atom - is allowed to interact with each of the three chromophores. The frontier molecular orbitals of the three chromophores - *p*-bromoaryl groups - are the antibonding combination between the π aryl orbital and the bromine p_z orbital, seen in Figure 3. The diabatic energies of the bridging group, H_N, and the three chromophores, H_{ArBr}, are on the diagonal of the model Hamiltonian (eq 10). The bridge is allowed to interact, or bond, to the chromophores through off-diagonal coupling elements, as seen in the matrix $\mathbf{H}_{unsym}$ (eq 12). The ground state in the diabatic basis corresponds to the hole in H_N, seen in Figure 5.

$$\mathbf{H_{unsym}} = \begin{bmatrix} H_N & \frac{V}{\sqrt{3}} & \frac{V}{\sqrt{3}} & \frac{V}{\sqrt{3}} \\ \frac{V}{\sqrt{3}} & H_{ArBr} & 0 & 0 \\ \frac{V}{\sqrt{3}} & 0 & H_{ArBr} & 0 \\ \frac{V}{\sqrt{3}} & 0 & 0 & H_{ArBr} \end{bmatrix} \quad (12)$$

The diabatic energies of the three chromophores are degenerate by interchange symmetry. Symmetry adapted linear combinations of the three chromophore orbitals can be made using the C_3 point group without breaking the degeneracy of the three diabats. There is one symmetric linear combination, H_A, and a pair of doubly degenerate linear combinations, H_E. The symmetric linear combination is of appropriate symmetry to interact with the bridge, as seen in $\mathbf{H_{sym}}$ (eq 13). The E linear combinations are not of appropriate symmetry to interact with nitrogen p_z orbital and consequently remain energetically equivalent to the diabatic energies H_{ArBr}.

$$\mathbf{H_{sym}} = \begin{bmatrix} H_N & V & 0 & 0 \\ V & H_A & 0 & 0 \\ 0 & 0 & H_E & 0 \\ 0 & 0 & 0 & H_E \end{bmatrix} \quad (13)$$

The symmetric linear combination and the bridge will interact to form a bonding (in phase) and antibonding (out of phase) combination; the adiabatic approximation gives the energies of the symmetric molecular orbitals, shown in Figure 5. The ground state in the adiabatic basis corresponds to the hole in the highest energy orbital, the antibonding combination. The extent of the energetic splitting depends on the magnitude of the coupling; a larger coupling will yield a larger splitting. The eigenvalues given by the adiabatic approximation are given in eq 14.

$$A_{1,2} = \frac{1}{2}(H_N + H_A \pm \sqrt{(H_N - H_A)^2 + 4V^2}) \quad (14)$$

The coupling in the effective coupling model is not the same as the coupling outlined in the neighboring orbital model. The three chromophores in the effective coupling model are coupled to each other; it is assumed that they are allowed to interact via the bridge. The coupling gives control over the exchange or "hopping" rate of the charge between the three chromophores in the excited state. The coupling in neighboring orbital model allows the chromophores to interact indirectly by coupling them to the bridge, not directly to each other.

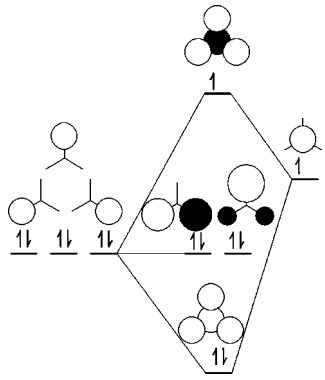

Figure 5. Simplified molecular orbital diagram for the neighboring orbital model. The bridge is mixed with the A linear combination of chromophore orbitals. The relative energy of the E linear combination is unchanged from the diabatic energy. The electron configuration for the ground state is shown for both the diabatic and adiabatic basis.

6. Transition Dipoles. In order to describe the electronic transition in the three-chromophore system, it is necessary to derive how the ground and excited electronic states are connected upon optical excitation. In the case of $[N(p\text{-}C_6H_4Br)_3]^+$, the charge in the ground state is delocalized over the entire compound. More charge is pushed onto the chromophores by the electric vector of light - giving the three unit vectors of the unsymmetrized transition dipoles. The magnitude of each transition dipole is equivalent as required by the interchange symmetry imposed on the system. It is possible that the charge localizes onto a single chromophore upon excitation. However, in the case of strongly interacting chromophores, as in $[N(p\text{-}C_6H_4Br)_3]^+$, it is more accurate to describe the wave packet as evolving on all three diabatic potential surfaces representing the *p*-bromoaryl groups, which interact with each other through the bridge.

The electronic absorption spectrum of the three-chromophore system is calculated using the time-dependent quantum wave packet propagation.[24] Since the three chromophores are allowed to interact with each other, it is necessary to know the phase relation between the chromophores as the charge "hops" between the chromophores across the bridge. The phase relation is important as it determines whether there is constructive or destructive interference between the wave packets and thus determines the selection rules and the vibrational fine structure.

The collected spectra are composed of an ensemble of randomly oriented molecules with respect to the electric vector of light; the calculated spectrum requires an average over all possible orientations. This procedure, outlined in the Supporting Information, indicates the initial phase relation required between any of the chromophores upon optical excitation. The result of the orientational averaging gives the autocorrelation function ($\langle\Phi|\Phi(t)\rangle$) that describes how the wave packets develop in time. The autocorrelation function reveals that the phase of the wave packet must change sign across the origin of the molecule.

The diabatic transition dipoles can be written in an infinite number of ways, just as the pair of doubly degenerate linear combinations can be displayed in an infinite number of ways. In keeping with the Cartesian coordinate system of the C_3 point group, a pair of dipole moment matrices, $\boldsymbol{\mu}^x$ and $\boldsymbol{\mu}^y$ (eq 14a), can be defined as the x and y vector components of the transition dipoles of each of the individual chromophores. The two dipole matrices can be symmetrized using the C_3 point group - the same transformation performed on $\mathbf{H_{unsym}}$. The symmetrized transition dipoles, $\boldsymbol{\mu}_{sym}{}^x$ and $\boldsymbol{\mu}_{sym}{}^y$ (eq 15), show the A → E transition is dipole allowed; the A → A transition is electronic dipole forbidden but vibronically allowed.

$$\boldsymbol{\mu}^y = \begin{pmatrix} 0 & 1 & \frac{-1}{2} & \frac{-1}{2} \\ 1 & 0 & 0 & 0 \\ \frac{-1}{2} & 0 & 0 & 0 \\ \frac{-1}{2} & 0 & 0 & 0 \end{pmatrix} \quad \boldsymbol{\mu}^x = \begin{pmatrix} 0 & 0 & \frac{\sqrt{3}}{2} & \frac{-\sqrt{3}}{2} \\ 0 & 0 & 0 & 0 \\ \frac{\sqrt{3}}{2} & 0 & 0 & 0 \\ \frac{-\sqrt{3}}{2} & 0 & 0 & 0 \end{pmatrix} \quad (14a)$$

$$\boldsymbol{\mu}_{sym}{}^y = \begin{pmatrix} 0 & 0 & \frac{\sqrt{6}}{2} & 0 \\ 0 & 0 & 0 & 0 \\ \frac{\sqrt{6}}{2} & 0 & 0 & 0 \\ 0 & 0 & 0 & 0 \end{pmatrix} \quad \boldsymbol{\mu}_{sym}{}^x = \begin{pmatrix} 0 & 0 & 0 & \frac{\sqrt{6}}{2} \\ 0 & 0 & 0 & 0 \\ 0 & 0 & 0 & 0 \\ \frac{\sqrt{6}}{2} & 0 & 0 & 0 \end{pmatrix} \quad (15)$$

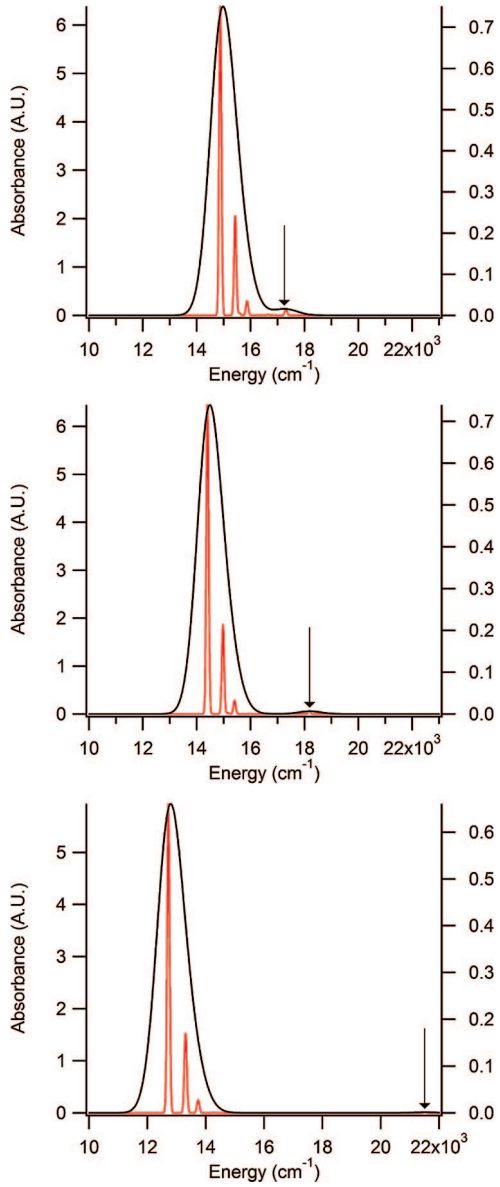

Figure 6. Calculated spectra using the effective coupling model: $H_{\mathrm{ef\,f}} = 500, 1000, 2700\ \mathrm{cm}^{-1}$; $\omega = 500$; $\Gamma = 30$ (red trace, sharp line; units on left axis), 300 cm^{-1} (black trace, broad band; units on right axis). The arrows point to the vibronically allowed A → A transition. Note that the allowed transition to the E state decreases in energy as the coupling is increased.

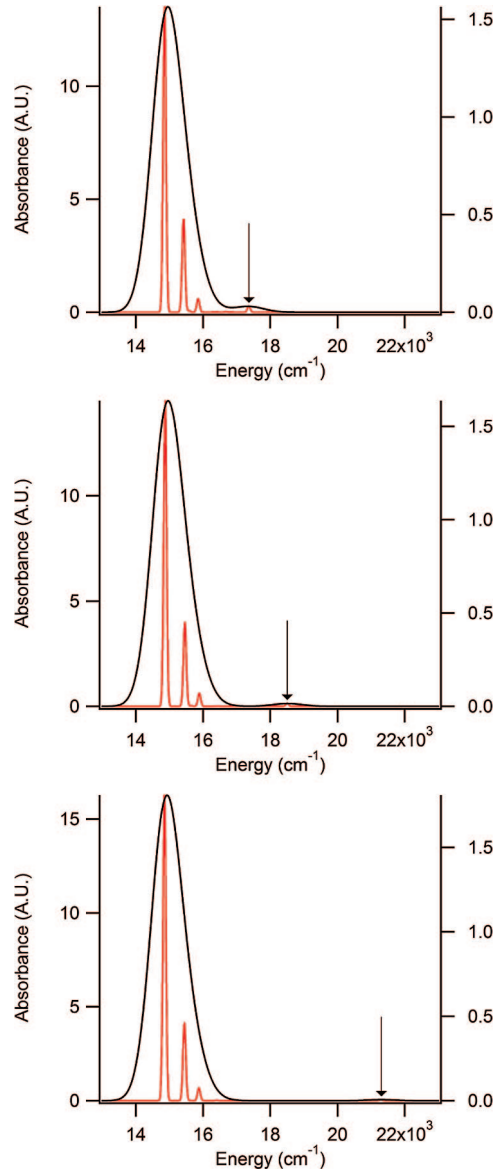

Figure 7. Calculated spectra using the neighboring orbital model: $V = 2530, 3530, 5530\ \mathrm{cm}^{-1}$; $\omega = 500$; $\Gamma = 30$ (red trace, sharp lines; units on left axis), 300 cm^{-1} (black trace, broad band; units on right axis). The arrows point to the vibronically allowed A → A transition. Note that the allowed transition to the E state remain fixed in energy.

7. Calculated Spectra from the Two Models. ***Effective Coupling Model.*** The electronic transition at 14 220 cm^{-1} can be modeled using either the effective coupling model or the neighboring orbital model. The effective coupling model possesses a single nondisplaced oscillator, representing the ground state with the charge localized on the nitrogen. The excited state is represented by three diabatic oscillators displaced according to the C_3 requirement and coupled to each other. The transition is modeled by a vertical transition of the ground-state wave packet onto the mixed valence excited state. The wave packet is placed with opposite phase onto two of the excited-state diabats with no intensity on the third—as the transition dipoles dictate. The spectrum is finally generated by allowing the wave packets to propagate in time on the mixed valence excited-state surfaces.

The sign and the magnitude of the effective coupling (H_{eff}) both influence the spectral results. The sign of the coupling influences the identity or relative energy of the adiabatic surfaces used in describing the system. The adiabat representing the A excited state is displaced by $+2H_{\mathrm{eff}}$ at the electronic origin. The adiabats representing the E electronic state are degenerate at the electronic origin and are displaced by $-H_{\mathrm{eff}}$. When modeling the spectra of $[\mathrm{N}(p\text{-}\mathrm{C_6H_4Br})_3]^+$ positive coupling is used as the E excited-state surfaces are closer in energy than A excited-state surface relative to the energy of the ground-state surface.

The influence of the magnitude of the effective coupling is displayed in Figure 6. As the magnitude of the coupling is increased, the energy separation between the E and A excited states increases. It is also observed that as the effective coupling increases the intensity of the vibronically allowed transition to the A excited state becomes weaker. The spectra calculated with low damping displayed in Figure 6 show vibrational fine structure, which broadens as the damping is increased. The vibrational fine structure observed in the E excited state is approximately $\hbar\omega$, where ω is the oscillator strength of the

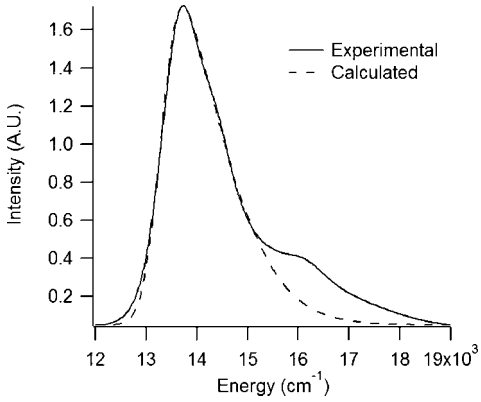

Figure 8. Fit of absorption spectrum by estimating distortions from the 676.4 nm excitation wavelength. A damping of 220 cm^{-1} and E_{00} of 13 490 cm^{-1} were used. The shoulder at 15800 cm^{-1} is assigned as the $A_{3,4}$ transition and is not included in this calculation.

diabats in the excited state, as is expected for a transition to the doubly degenerate electronic state.[38]

Neighboring Orbital Model. The neighboring orbital model Hamiltonian can also be used to model the three-chromophore system. In this model there are four diabatic surfaces: three diabats are energetically degenerate - representing the chromophores - and the fourth diabat is energetically displaced - representing the bridge. The chromophore diabats are displaced from the electronic origin according to the C_3 point group; the bridge diabat is centered at the electronic origin. Each of the three chromophore diabats is coupled to the bridge diabat, but not to each other. The ground-state eigenfunction corresponds to the odd electron (or equivalently the hole) residing in the highest energy orbital and is calculated using the four coupled diabats. The transition is modeled by multiplying the ground-state eigenfunction by the unsymmetrized transition dipole matrix, section 6, and propagating in time. Including the on-diagonal portion of the transition dipole moment only affects the total intensity of the spectrum; the absolute intensity is not being considered, so the on-diagonal portion is neglected.

The magnitude of the coupling influences the spectra in a manner similar to that of the effective coupling model. Increasing the coupling causes the energy spacing between the E and A excited states to increase, as shown in Figure 7. As the magnitude of the coupling increases, the intensity of the vibronically allowed transition to the A excited state also becomes weaker. The sign of the coupling has no influence on the spectrum.

The effect that the coupling has on the adiabatic energy levels is different from that of the effective coupling model. The neighboring orbital model correctly reproduces the prediction that the two E adiabats remain energetically equivalent to the diabatic energies of the charge-bearing units and the two A states split in energy. The effective coupling model fails to reproduce the prediction that the two E states remain energetically equivalent to the diabatic energies of the charge-bearing units; both the E and A excited states are split away from the diabatic energies of the charge-bearing units. The vibronic bands calculated by both models are remarkably similar; both display a vibrational spacing of $\hbar\omega$ due to the symmetric component of the electronic motion.

Fitting the spectrum requires the use of all of the displaced normal modes observed in the resonance Raman spectrum. A good fit (Figure 8) was obtained by using similar distortions estimated from Savin's formula with the exception of the 672 cm^{-1} mode that required a larger delta. This mode probably cannot be modeled by a displaced harmonic potential with no change in force constant. The most highly distorted normal mode (282 cm^{-1}) corresponds to a ring rocking as expected for the formal nitrogen p nonbonding orbital to the nitrogen-C_6H_4Br pi antibonding orbital transition that weakens the N−C pi interaction.

Summary

The excited-state mixed valence transition for three-chromophore systems can be modeled using either an effective coupling model or a neighboring orbital model. The models were explored using tris(4-bromophenyl)amine as an instructive example. The three chromophores are directly coupled to each other in the "effective coupling model" resulting in a splitting of three times the effective coupling between the excited state adiabats. In the "neighboring orbital model" the three chromophores are coupled to the bridge. The adiabats representing the E excited state are energetically equivalent to the chromophore diabatic energy. The extent of the splitting between the two A adiabats depends on the magnitude of the coupling. Both the effective coupling model and the neighboring orbital model yield similar results with respect to the dipole and vibronically allowed electronic transitions as well as the vibrational fine structure. The major significant difference is that in the neighboring orbital model the E states remain unshifted in energy with respect to the diabatic energies of the chromophores, which is where the effective coupling model breaks down. The lowest energy transition in the absorption spectrum is assigned as an electronic transition from the HOMO to the SOMO using Gaussian 03.[34] The absorption spectrum was calculated with the time-dependent theory of spectroscopy using all of the resonantly enhanced Raman modes. The most highly distorted normal mode corresponds to a ring rocking as expected for the formal nitrogen p nonbonding orbital to the nitrogen-C_6H_4Br pi antibonding orbital transition that weakens the N−C pi interaction.

Acknowledgment. We thank the National Science Foundation for support of this work under CHE-0204197 (SFN), CHE-0647719 (SFN), and CHE-0809384 (JIZ).

Supporting Information Available: Molecular orbital drawings of $[N(p\text{-}C_6H_4Br)_3]^+$ from Koopmans-based calculations; orientational averaging results for an arbitrary planar three-chromophore system. This material is available free of charge via the Internet at http://pubs.acs.org..

References and Notes

(1) (a) Lockard, J. V.; Zink, J. I.; Konradsson, A. E.; Weaver, M. N.; Nelsen, S. F. *J. Am. Chem. Soc.* **2003**, *125*, 13471–13480. (b) Lockard, J. V.; Zink, J. I.; Trieber, D. A., II; Konradsson, A. E.; Weaver, M. N.; Nelsen, S. F *J. Phys. Chem. A,* **2005**, *195*, 1205–1215. (c) Lockard, J. V.; Valverde, G.; Neuhauser, D.; Zink, J. I.; You, L.; Weaver, M. N.; Nelsen, S. F *J. Phys. Chem. A* **2006**, *110*, 57–66.

(2) Cannon, R. D; Ladda, M.; Brown, D. B; Marshall, K. M.; Elliott, C. M. *J. Am. Chem. Soc.* **1984**, *106*, 2591–2594.

(3) Bonvoisin, J.; Launay, J.-P.; Van der Auweraer, M.; De Schryver, F. C. *J. Phys. Chem.* **1994**, *98*, 5052–5057.

(4) Bonvoisin, J.; Launay, J.-P.; Verbouwe, W.; Van der Auweraer, M.; De Schryver, F. C. *J. Phys. Chem.* **1996**, *100*, 17079–17082.

(5) Haga, M.-A.; Ali, M. M.; Sato, H.; Monjushiro, H.; Nozaki, K.; Kano, K *Inorg. Chem.* **1998**, *37*, 2320–2324.

(6) Lambert, C.; Gaschler, W.; Schmälzlin, E.; Meerholz, K.; Braäuchle, C. *J. Chem Soc., Perkin Trans. 2* **1999**, 577–588.

(7) Lambert, C.; Nöll, G.; Hampel, F. *J. Phys. Chem. A* **2001**, *105*, 7751–7758.

(8) Lambert, C. *Chem. Phys. Chem.* **2003**, *4*, 877–880.

(9) Selby, T. D.; Blackstock, S. C. *Org. Lett.* **1999**, *1*, 2053–2055.

(10) Rathore, R.; Burns, C. L.; Deseinicu, M. I. *Org. Lett.* **2001**, *3*, 2887–2890.
(11) Lambert, C.; Nöll, G. *Angew. Chem., Int. Ed.* **1998**, *37*, 2107–2110.
(12) Lambert, C.; Nöll, G. *Chem. Eur. J.* **2002**, *8*, 3467–3477.
(13) Rathore, R.; Burns, C. L.; Abdelwahed, S. A. *Org. Lett.* **2004**, *6*, 1689–1692.
(14) Chebny, V. J.; Shukla, R.; Rathore, R. *J. Phys. Chem. A* **2006**, *110*, 13003–13006.
(15) Chebny, V. J.; Dhar, D.; Lindeman, S. V.; Rathore, R. *Org. Lett.* **2006**, *8*, 5041–5044.
(16) Sun, D.; Rosokha, S. V.; Kochi, J. K. *Angew. Chem., Int. Ed.* **2005**, *44*, 5133–5136.
(17) Rosokha, S. V.; Neretin, I. S.; Sun, D.; Kochi, J. K. *J. Am. Chem. Soc.* **2006**, *128*, 9394–9407.
(18) Wieland, H. *Chem. Ber.* **1907**, *40*, 4260.
(19) (a) Weitz, E.; Schwechten, H. W. *Chem. Ber.* **1926**, *59*, 2307. (b) Weitz, E.; Schwechten, H. W. *Chem. Ber.* **1927**, *60*, 545.
(20) (a) Baker, T. N., III; Doherty, W. P., Jr.; Kelley, W. S.; Newmeyer, W.; Rogers, J. E., Jr.; Spalding, R. E.; Walter, R. I. *J. Org. Chem.* **1965**, *30*, 3714–3718. (b) Kelley, W. S.; Monack, L.; Rogge, P. T.; Schwartz, R. N.; Varimbi, S. P.; Walter, R. I. *Liebigs Ann. Chem.* **1971**, *744*, 129. (c) Allendoerfer, R. D.; Smith, G.; Walter, R. I. *J. Phys. Chem.* **1968**, *72*, 1217–1222. (d) Walter, R. I. *J. Am. Chem. Soc* **1966**, *88*, 1923–1930. (e) Walter, R. I.; Codrington, R. S.; D'Adamo, F. R.; Torrey, H. C. *J. Chem. Phys.* **1956**, *25*, 319–324. (f) Hagopian, L.; Koehler, G.; Walter, R. I. *J. Phys. Chem.* **1967**, *71*, 2290–2296. (g) Linkletter, S. J. G.; Pearson, G. A.; Walter, R. I. *J. Am. Chem. Soc.* **1977**, *99*, 5269–5272. (h) Pearson, G. A.; Walter, R. I. *J. Am. Chem. Soc.* **1977**, *99*, 5262–5268. (i) Pearson, G. A.; Rocek, M.; Walter, R. I. *J. Phys. Chem.* **1978**, *82*, 1185–1192. (j) Brown, G. M.; Freeman, G. R.; Walter, R. I. *J. Am. Chem. Soc.* **1977**, *99*, 6910–6915.
(21) Connelly, N. G.; Geiger, W. E. *Chem. Rev.* **1996**, *96*, 877–910.
(22) Earle, M. J. Tris(4-bromophenyl)aminium hexachloroantimonate. In *Encyclopedia of Reagents for Organic Synthesis*; Paquette, L. A. , Ed.; Wiley: New York, 1995; Vol. 8, p 5427.
(23) Mahboob, M.; Sundheim, B. R. *Theor. Chim. Acta* **1968**, *10*, 222.
(24) (a) Lee, S.-Y.; Heller, E. J. *J. Chem. Phys.* **1979**, *71*, 4777–4788. (b) Heller, E. J. *Acc. Chem. Res.* **1981**, *14*, 368–375. (c) Heller, E. J.; Sundberg, R. L.; Tannor, D. *J. Phys. Chem.* **1982**, *86*, 1822–1833.
(25) Clark, R. J. H.; Dines, T. J. *Angew. Chem., Int. Ed. Engl.* **1986**, *25*, 131.
(26) (a) Myers, A. B.; Mathies, R. A. *Biological Applications of Raman Spectroscopy*; Wiley-International: New York, 1987; Vol. 2, p 1. (b) Myers, A. B. *Laser Techniques in Chemistry*; Wiley: New York, 1995; Vol. 23, p 325. (c) Myers, A. B. *Acc. Chem. Res.* **1997**, *30*, 519–527.
(27) (a) Shin, K. S. K.; Zink, J. I. *Inorg. Chem.* **1989**, *28*, 4358–4366. (b) Zink, J. I.; Shin, K. S. K. *Advances In Photochemistry*; Wiley: New York, 1991; Vol. 16, p 119. (c) Shin, K. S. K.; Zink, J. I. *J. Am. Chem. Soc.* **1990**, *112*, 7148–7157.
(28) Bally, T. In *Radical Ionic Systems*; Lund, A., Shiotani, M. , Eds.; Kluwer: Dortrecht, 1991; pp 3−54.
(29) (a) Hoijtink, G. J.; Weijland, W. P. *Recl. Trav. Chim.* **1957**, *76*, 836–838. (b) Buschow, K; J, J.; Dieleman, J.; Hoijtink, G. J. *Mol. Phys.* **1963−1964**, *7*, 1–9.
(30) Nelsen, S. F.; Weaver, M. N.; Telo, J. P.; Zink, J. I. *J. Am. Chem. Soc.* **2005**, *127*, 10611–10622.
(31) Nelsen, S. F; Weaver, M. N.; Telo, J. P.; Lucht, B. L.; Barlow, S. *J. Org. Chem.* **2005**, *70*, 9326–9333.
(32) Nelsen, S. F.; Luo, Y.; Weaver, M. N.; Lockard, J. V.; Zink, J. I. *J. Org. Chem.* **2006**, *71*, 4286–4295.
(33) Nelsen, S. F.; Weaver, M N.; Bally, T.; Yamazaki, D.; Komatsu, K.; Rathore, R. *J. Phys. Chem. A* **2007**, *111*, 1667–1676.
(34) Frisch, M. J.; Trucks, G. W.; Schlegel, H. B.; Scuseria, G. E.; Robb, M. A.; Cheeseman, J. R.; Montgomery, J.; Vreven, T.; Kudin, K. N. ; Burant, J. C.; Millam, J. M.; Iyengar, S. S.; Tomasi, J.; Barone, V.; Mennucci, B.; Cossi, M.; Scalmani, G.; Rega, N.; Petersson, G. A.; Nakatsuji, H.; Hada, M.; Ehara, M.; Toyota, K.; Fukuda, R.; Hasegawa, J.; Ishida, M.; Nakajima, T.; Honda, Y.; Kitao, O.; Nakai, H.; Klene, M.; Li, X.; Knox, J. E.; Hratchian, H. P.; Cross, J. B.; Adamo, C.; Gomperts, J. J. R.; Stratmann, R. E.; Yazyev, O.; Austin, A. J.; Cammi, R.; Pomelli, C.; Ochterski, J. W.; Ayala, P. Y.; Morokuma, K.; Voth, G. A.; Salvador, P.; Dannenberg, J. J.; Zakrzewski, V. G.; Dapprich, S.; Daniels, A. D.; Strain, M. C.; Farkas, O.; Malick, D. K.; Rabuck, A. D.; Raghavachari, K.; Foresman, J. B.; Ortiz, J. V.; Cui, Q.; Baboul, A. G.; Clifford, S.; Cioslowski, J.; Stefanov, B. B. G.; Liu, A. L.; Piskorz, P.; Komaromi, I.; Martin, R. L.; Fox, D. J.; Keith, T.; Al-Laham, M. A.; Peng, C. Y.; Nanayakkara, A.; Challacombe, M. ; Gill, P. M. W.; Johnson, B.; Chen, W.; Wong, M. W.; Gonzalez, C.; Pople, J. A. *Gaussian 03; Revision B.05 ed.*; Gaussian, Inc.: Pittsburgh, PA, 2003.
(35) Zhang, J. Z.; Heller, E. J.; Huber, D.; Imre, D. G. *J. Phys. Chem.* **1991**, *95*, 6129–6141.
(36) (a) Reber, C.; Zink, J. I. *J. Chem. Phys.* **1992**, *96*, 2681–2690. (b) Talaga, D. S.; Zink, J. I. *J. Phys. Chem.* **1996**, *100*, 8712–8721. (c) Wootton, J. L.; Zink, J. I. *J. Am. Chem. Soc.* **1997**, *119*, 1895–1900. (d) Henary, M.; Zink, J. I. *J. Am. Chem. Soc.* **1989**, *111*, 7407–7411. (e) Zink, J. I. *Inorg. Chem.* **1973**, *12*, 1957.
(37) Nelsen, S. F.; Weaver, M. N.; Pladziewicz, J. R.; Ausman, L. K.; Jentsch, T. L.; O'Koneck, J. J. *J. Phys. Chem. A* **2006**, *110*, 11665.
(38) (a) Longuet-Higgins, H. C.; Opik, U.; Pryce, M. H. L. F. R. S.; Sack, R. A. *Proc. R. Soc. London, Ser. A, Mat. Phys. Sci.* **1958**, *244*, 1–16. (b) Bersuker, I. B.; Polinger, V. Z. *Vibronic Interaction in Molecules and Crystals*; Springer: Berlin, 1989; Vol. 49.

JP807940H